Scanning tunneling microscopy

by G. Binnig H. Rohrer

Presented here is an overview of the present status and future prospects of scanning tunneling microscopy. Topics covered include the physical basis of the scanning tunneling microscope, its instrumentation aspects, and its use for structural and spectroscopic imaging—on a scale which extends to atomic dimensions. Associated experimental and theoretical studies are reviewed, including several which suggest potential applicability of this new type of microscope to a relatively broad range of biological, chemical, and technological areas.

1. Introduction

In the past several years, scanning tunneling microscopy (STM) has developed into an imaging method with diverse possibilities for real-space imaging on a scale which extends to atomic dimensions. (Note: The designation "STM" is subsequently used interchangeably to denote "scanning tunneling microscopy" and "scanning tunneling microscope.") The original purpose of the work on the STM was to develop a means of imaging the structure and electrical properties of insulating layers thin enough to permit electron tunneling [1]. Thus, the STM was meant to be suitable for imaging not only the structure of such an insulating layer but also its local conductivity. This local probing capability, combined with its adaptability to various

[®]Copyright 1986 by International Business Machines Corporation. Copying in printed form for private use is permitted without payment of royalty provided that (1) each reproduction is done without alteration and (2) the *Journal* reference and IBM copyright notice are included on the first page. The title and abstract, but no other portions, of this paper may be copied or distributed royalty free without further permission by computer-based and other information-service systems. Permission to *republish* any other portion of this paper must be obtained from the Editor.

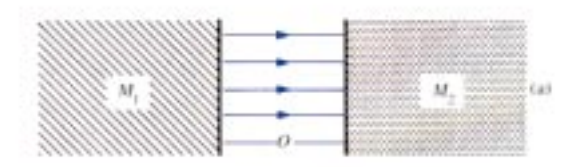
environments, and the tunable, low electron energies which it utilizes, make it increasingly attractive for use in diverse areas of science and technology, reaching beyond its initial use in atomic-scale imaging. In many applications, its primary role is to perform a local experiment in which imaging is used primarily to select and define the location of the experiment. In other applications, such as, for example, local displacement monitoring, imaging might not be used at all. Although most of the STM applications examined thus far have dealt with structural microscopy, many others are now in the exploration stage.

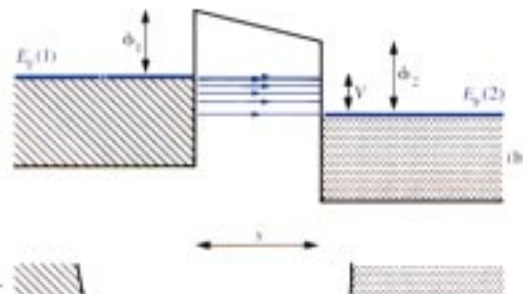
Historically, when electron tunneling was first proposed in the late twenties [2], it was envisaged in connection with vacuum barriers. Its first experimental realization, however, was achieved with solid barriers about thirty years later [3], vacuum barriers having been discarded as being impractical [4]. Later attempts to perform vacuum tunneling per se and in scanning configurations did not advance sufficiently to allow the development of an operational STM [5]. Except for the Topographiner, as developed by Young, Ward, and Scire [5], the primary interest was in performing tunneling spectroscopy in the absence of a native oxide barrier.

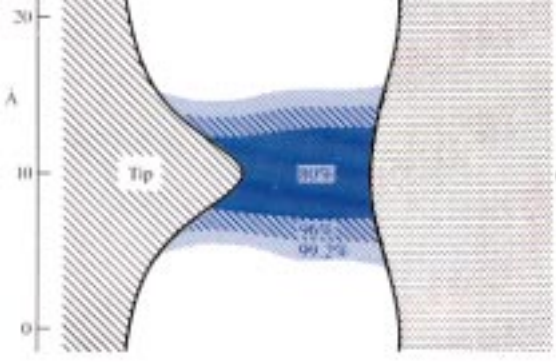
The papers in this and the next issue of the *IBM Journal* of *Research and Development* are based on contributions presented at the first workshop [6] on this subject. They reflect the present state of the art and the increasing applicability of the STM to diverse areas of interest. The purpose of this paper is to provide an introduction to the subsequent papers in this and the next issue of the *Journal*, and to review the evolution of the STM and associated studies carried out during the past several years.

2. Physical basis and modes of operation

The underlying physical basis of the STM is electron tunneling. For its theory and applications in solid-state







(a) Planar metal-oxide-metal junction $(M_1\text{-}O\text{-}M_2)$. The current density, indicated by the red lines, is uniform. (b) Illustrative energy diagram for a tunneling junction having a trapezoidal barrier (ϕ_1,ϕ_2) of thickness s. As indicated, only electrons tunneling from states between $E_F(1)$ and $E_F(1) - V$ in M_1 to unoccupied states between $E_F(2)$ and $E_F(2) + V$ in M_2 contribute to the tunneling current. The current density (per unit energy) is highest at $E_F(1)$. (c) Calculated current density distribution for tunneling from a tip to a corrugated surface, assuming an effective barrier height of 2.41 eV, a tip radius of 1.7 Å, and s = 4 Å (after [11]).

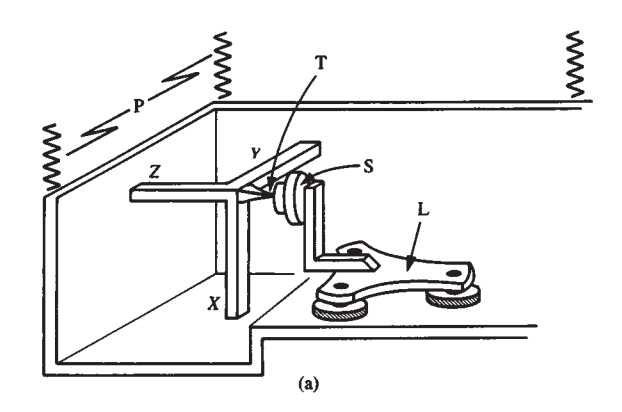
physics, we refer the reader to the vast amount of literature on that subject [7–9]. Here, we summarize the essential ingredients necessary for understanding the operation of the STM and developing an appreciation of its key features.

Electron tunneling occurs between two conductors separated by a sufficiently thin insulating layer or, in physical terms, potential barrier. In the transfer-Hamiltonian approach [10], the tunneling current I is a measure of the overlap in the separating gap (or intervening insulator) of the wave functions of the two electrodes. Therefore, I is a function of the electrode separation and the nature of the electronic states involved. The most common tunneling junction consists of a planar conductor-insulator-conductor sandwich in which the insulator is usually an oxide layer

formed by oxidation of one of the electrodes [see Figure 1(a)]. For free electrons tunneling through a planar barrier at small voltages $V \ll \phi$, the current density, j, can be written as [7]

$$j = (e^2/\hbar) \cdot (\kappa_0/4\pi^2 s) \cdot V \cdot \exp(-2\kappa_0 s), \tag{1}$$

where s is the effective tunnel distance in Å, κ_0 the inverse decay length of the wave-function density outside the surface, V the applied voltage in volts, and $(e^2/h) = 2.44 \cdot 10^{-4} \,\Omega^{-1}$; κ_0 is given by the expression $2\kappa_0$ (Å) = $1.025\sqrt{\phi(eV)}$, with ϕ the effective barrier height [$\approx (\phi_1 + \phi_2)/2$]. In the following, the factor 1.025 is replaced by 1, distances and energies are given in units of Å and eV, respectively, and voltage (in volts) or energy (in eV) are designated as V. The effective barrier height of a vacuum gap between the two electrodes is, to a first approximation, the average of the two respective work functions; most often a



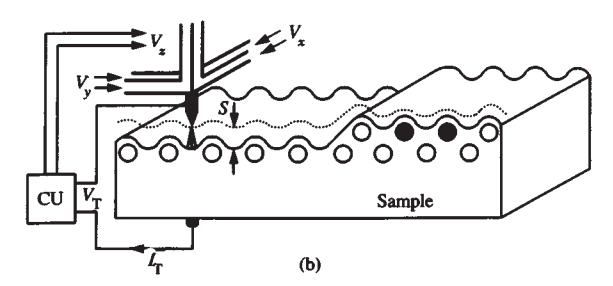


Figure 2

Schematic of a scanning tunneling microscope and its operation. The tip T of the microscope depicted in (a) is scanned over the surface of a sample S with a piezoelectric tripod (X,Y,Z). The rough positioner L brings the sample within reach of the tripod. A vibration filter system P protects the instrument from external vibrations. In the constant tunneling current mode of operation, a voltage V_z is applied to the Z piezoelectric element by means of the control unit CU depicted in (b) to keep the tunneling current constant while the tip is scanned across the surface by altering V_x and V_y . The trace of the tip, a y-scan, generally resembles the surface topography. Electronic inhomogeneities also produce structure in the tip trace, as illustrated on the right above two surface atoms having excess negative charge.

few eV. Oxide barrier heights are considerably smaller, usually below 1 eV. Figure 1(b) shows an energy-distance schematic of a typical metal-oxide-metal tunneling junction. At higher voltages, the effective barrier height in (1) becomes a function of V[7]. In the case of non-free electrons and non-planar barriers, the total current I can no longer be expressed in such a simple and closed form. Nevertheless, we still have essentially an exponential dependence of I on some effective tip-surface separation and barrier height. But the prefactor is altered because of density-of-state effects. The electrons close to the Fermi level $E_{\rm F}(1)$ [in conjunction with the empty states at $E_{\rm F}(2) + V$] contribute most effectively to the tunneling current since they experience the smallest effective barrier height. The resulting energy selectivity is reflected in the current-voltage characteristic, and is of prime interest in the classical type of electron tunneling spectroscopy which is performed on conductor-insulatorconductor sandwich junctions [8, 9]. Tunneling spectroscopy thus gives access to the density of both occupied and empty states.

Basic to the operation of the STM is the extreme sensitivity to tunneling distance of the tunneling current. If one electrode is formed into the shape of a tip, the tunneling current is confined to a filament between the apex of the tip and the surface or object under investigation [see Figure 1(c)]. The tunneling current decreases by roughly an order of magnitude for every distance increase by 1 Å, and the effective diameter of the filament, $L_{\rm eff}$, can become extremely small for a pointed tip. In the case of a single atom at the apex, $L_{\rm eff}$ decreases to a magnitude of atomic dimension. By using vacuum, gas, or a liquid as the tunneling barrier between tip and surface, the tip and thus the tunneling current filament can be scanned freely across the surface. A possible STM, which uses a piezoelectric tripod for fine-positioning of the tip, is depicted in Figure 2(a). By adjusting the z-position of the tip, to keep the tunneling current constant, contours of constant tunneling current can be obtained, as illustrated in Figure 2(b). On a surface with uniform electronic properties, this procedure yields an image of the surface topography, folded with the instrumental resolution. As an example, in Figure 3 we show an STM image of a clean Au(100) surface exhibiting atomically flat terraces with monolayer step lines [12]. On an electronically inhomogeneous surface, the change which occurs in the tunneling current upon moving the tip laterally depends not only on the topography but also on the local electronic structure. The central problem in taking and understanding an STM image is, then, how to disentangle the richness of information it contains into its topographic, chemical, and electronic features.

This imaging process is quite similar to Stylus Profilometry [13]. The stylus, carried by a cantilever beam, traces the sample surface with a constant loading force. The result is a topographical image in the 1000-Å lateral and

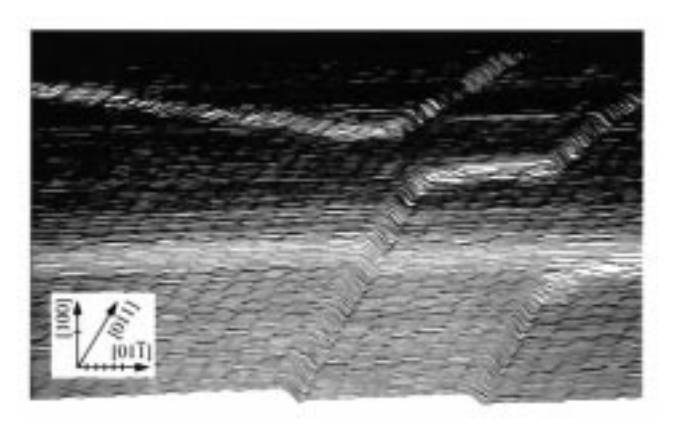


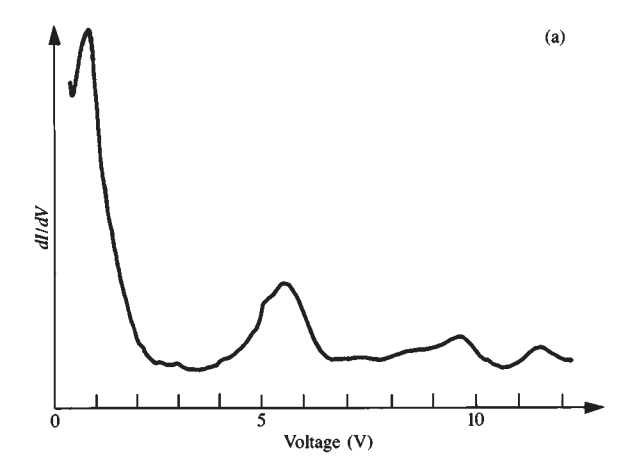
Figure 3

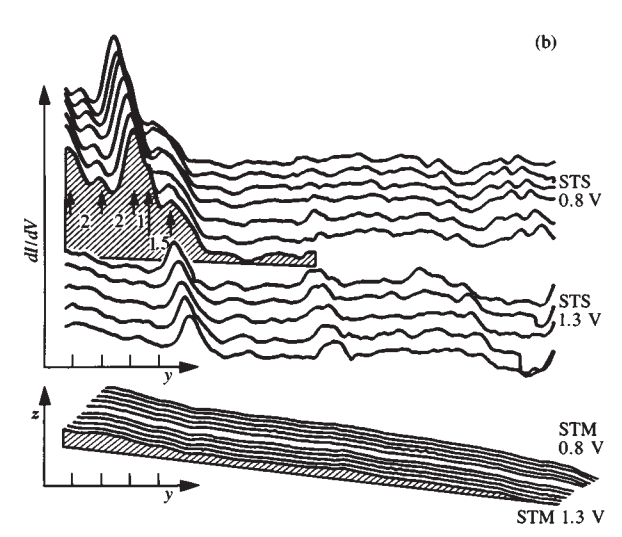
STM image of a clean Au(100) surface obtained at a constant tunneling current of 1 nA, showing flat terraces and monolayer step lines. The wavy structure is real and can be resolved into individual atomic rows. The divisions on the axes correspond to spacings of $5 \, \text{Å}$. (From [12], reproduced with permission.)

10-Å vertical resolution range, provided the mechanical surface properties are uniform. Hardness inhomogeneities, for instance, have an effect on the topographical image of the stylus which is analogous to that of electronic inhomogeneities in STM.

Electronic and chemical surface properties manifest themselves primarily in the voltage dependence of the tunneling current. They appear as specific features in the local I-V, V-s, or I-s characteristics. In practice, electronic or chemical images are obtained by recording dI/dV or dI/ds while scanning and controlling the gap width by keeping the average current constant. Depicted in Figure 4 is an example of such scanning tunneling spectroscopic (STS) imaging [14]. (Note: The designation "STS" is subsequently used interchangeably to denote "scanning tunneling spectroscopic" and "scanning tunneling spectroscopy.") In (a), the strong peak at 0.8 V is attributed to surface nickel oxide. In (b), the surface is imaged with respect to that spectroscopic feature (top) and I = constant (bottom). Whereas the STS images differ dramatically, the STM images remain unchanged. Because of the usually close relation of the tip-to-sample spacing at I = constant with the topography, of dI/dV with the local density of states, and of dI/ds with the local barrier height (or work function), associated images are often referred to as topographical or STM images, spectroscopic or STS images, and workfunction profiles, respectively. However, there are other ways to image a surface or object with the STM.

An important aspect of the STM is its apparent nondestructive nature, viz., no perceptible irreversible damage occurs as a result of its use. Reversible local changes on the surface induced by the vicinity of the tip or by the





Spectroscopic and structural imaging of NiO on a Ni(100) surface. Shown in (a) is dI/dV vs. V from an oxide-covered region. The strong peak at 0.8 V is characteristic of NiO. The STS and STM images shown in (b) were obtained at indicated bias voltages of 0.8 and 1.3 V. An oxide island to the left is evident in the STS image obtained at 0.8 V. Spatial separations in units of the NiO lattice spacings are indicated at the left. The oxide island is hardly noticeable in the STM images. The divisions on the y and z axes correspond to spacings of 5 Å. (From [14], reproduced with permission.)

high local electrical fields cannot be ruled out [15]. Their influence can be estimated by measuring at different currents or voltages. No evidence of appreciable reversible local disturbances exists in experiments reported so far. In addition, STM can be performed without appreciably altering surface electric fields. This simply requires application of a tunneling voltage which is equal and opposite to the contact potential $[\phi_1 - \phi_2]$ in Figure 1(b)]. On the other hand, the STM can be used to intentionally induce permanent local structural or chemical modifications.

Possibilities range from spurring chemical processes selectively by appropriate choice of electron energy or field strength to producing structural alterations caused by impact of the tip on the surface. Finally, the STM can be used as a local position-control or displacement-monitoring system. Before presenting some specific imaging and non-imaging examples, we briefly discuss some aspects and problems of STM instrumentation.

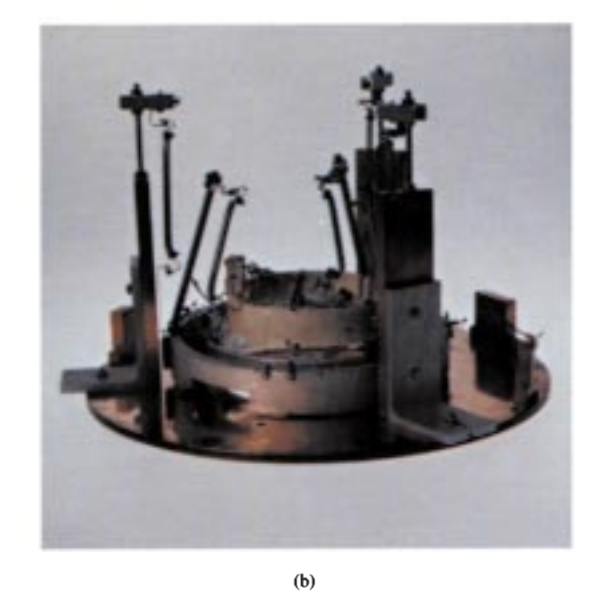
3. Instrumentation

The major instrumental problems to be overcome in an STM are those associated with the sharpness and the physical and chemical stability of the tunneling tip, and those associated with the mechanical stability of the width of the tunneling gap. Tip sharpness is the primary factor which determines the lateral resolution. The overall stability of the gap determines the vertical resolution and the quality of the tunneling spectra which are obtained. Considerations regarding gap-width stability are discussed in more detail by Pohl elsewhere in this issue [16]. The status and prospects of fabricating ultrasharp and stable tips are treated by Fink [17].

The gap-width stability is mainly limited by vibrations transmitted to the tunneling unit or created in the scanning process itself. Particularly detrimental are vibrations which can excite mechanical eigenmodes of the unit or parts thereof which affect the path connecting the tip with the sample. The influence of external vibrations is reduced by use of a vibration-isolation system; that of internal vibrations is reduced by mechanical rigidity and an electrical low-pass filter in the tip-position control loop limiting tip motion to frequencies below the lowest mechanical eigenfrequency. The latter obviously also limits the imaging speed on rough surfaces. Smooth surfaces with corrugation amplitudes less than the average tunneling distance can also be imaged by recording the tunneling-current deviations instead of the z-displacement of the tip [18]. The imaging speed is then limited by scanning speed and other factors related to the electronics of the system or the data-acquisition rate.

The photographs in Figure 5 depict the development of STM instrumentation in our laboratory. In the first-generation instrument, isolation of the tunneling gap from external vibrations was achieved by superconducting levitation [19]; in the second [1] and third [20] generations, by two-stage spring systems. Additional eddy-current damping with permanent magnets was used in all three generations. In the fourth generation [21], vibration isolation is achieved by using only viton dampers. A short account of what has been done with the various instruments is given in [21]. In this class of instruments, in addition to isolating the tunneling gap from external vibrations by some form of vibration-isolation system, rough positioning is achieved with "louse"-type piezoelectric configurations [1], magnetic accentuators [22, 23], or a differential screw with a reduction







(c)

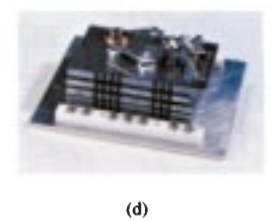


Figure 5

Photographs of the four generations (a) to (d) of STMs which have been used in our laboratory. Each is approximately 1/5 actual size.

lever system [24]. In another approach, the tunneling gap is rendered vibration-insensitive by making the mechanical connection between tip and sample very rigid, thus pushing the mechanical eigenmodes to frequencies far above those of significant external vibrations. A first step in this direction was the development of the squeezable tunneling junction [25], which, however, lacks scanning capability. STMs based on increased stiffness have been described in several contributions [26-28]. A hybrid of an STM and squeezable tunneling junction [27] operates even when immersed in liquid nitrogen. In another type of STM, use is made of bender elements for large excursions at low voltages [29]. In general, vibration protection is a compromise between great stiffness and the convenience of remote rough sample positioning over a range extending to several mm. Preference for either is dictated by the application in mind.

The sharpness and stability of the tip determine lateral resolution and reproducibility. Grinding or etching of tungsten wires (other materials such as stainless steel, gold, and iridium have also been used) appears thus far to be the standard method of obtaining workable tips for achieving atomic resolution. Further in situ sharpening is often required, in particular after unintentional contact of tip and sample, which can produce mechanically unstable whiskers on the tip, leading to unstable tunneling gaps. Small whiskers can be "blown off" by applying up to +100 volts to the tip, larger ones by heating and melting with currents up to a few μ A [1, 30–33]. For structures with known periodicity or known shape, such as a step, the image itself provides an indication of the tip sharpness. Even in these cases, an a priori knowledge of the detailed tip geometry is desirable, since STM structures appear as a combined image of the actual structure and the tip geometry [34]; e.g., symmetric structures imaged with an asymmetric tip appear asymmetric.

For high-resolution imaging of nonperiodic surface features of unknown size—one of the significant virtues of the STM—a predetermined tip geometry is obviously even more important and also may help to enhance the resolution by deconvolution procedures. Thus, the fabrication of well-defined, stable tips has become a central instrumental issue in STM. The ultimate goal is a symmetric tip with a distinct single electronic state from (or to) which the tunneling would occur. Preparation techniques borrowed from field-ion microscopy provide us with such tips [17].

A final point concerns the calibration of the piezoelectric drives. Calibration with a capacitance dilatometer [35] was found to yield two types of response to an applied voltage: an intrinsic, fast response <<1 s, limited by the electronics of the dilatometer, and a slow, domain-wall-motion response in the several-minute range with a time-integrated dilatation roughly equal to the intrinsic response. The latter can result in a troublesome distortion of images. An extended, relevant calibration study has recently been carried out by Vieira [36]

for a variety of piezoelectric ceramic materials at temperatures down to 4 K.

Because of the rapid progress in instrumentation, it is anticipated that by the time this paper appears, STMs will be smaller, more versatile, and less sensitive to vibrations, and will function more rapidly than at present.

4. Imaging structures: Experiments and theory

There are now abundant examples of surface-structure STM images. In surface-science applications, atomic resolution and ultrahigh vacuum have been of primary interest [1, 12, 18, 32, 37-43]. Early investigations in which atomic resolution was achieved in the imaging of surface reconstructions aroused the interest of many experimenters and motivated the first associated theoretical work. The two theoretical approaches, use of the transfer Hamiltonian [44, 45] and the direct-transmission approach [11, 46], provided the first insights regarding the physical basis for STM imaging and the associated lateral resolution which could be achieved. Merits and shortcomings of the two approaches and useful approximate treatments are discussed by Baratoff [47]. In the transfer-Hamiltonian approach, the tunneling tip is regarded as tracing contours of constant wave-function density, evaluated at the center of the (assumed) spherical tip, as it traverses a sample surface in the constant-current mode. The transmission approach does not relate STM images to such simple, physical concepts, but it provides an instructive view of the current distribution in the tunneling filament. Both approaches lead to similar expressions for the lateral resolution [24, 48]. In particular, the minimum periodicity, a_{m} , of a sinusoidal surface corrugation with amplitude c_s to be resolved is, for free electrons,

$$a_{\rm m} = \sqrt{\pi/\ln A} \cdot L_{\rm eff} \lesssim \pi \sqrt{2/\ln A} \cdot \sqrt{r + s/\phi^{1/4}}, \tag{2}$$

where r is the radius of curvature of the tip, s is the average width of the tunneling gap, ϕ is the effective barrier height, $A = c_s/c_d$, with c_d the smallest observable corrugation of the equicurrent surface traced by the tip (or, in effect, the gapwidth stability), and L_{eff} is the effective diameter of the tunneling current filament. The dominant factors are tip radius, gap width, and barrier height; the vertical stability enters only logarithmically. Equation (2) is expected to be a good approximation for a tip for which the jellium concept is meaningful, i.e., a metal tip with a radius of curvature of, say, 7 Å or more. Not taken into account are image potential and nonuniform barrier heights. The former drastically decreases ϕ at small gap widths and thus affects the resolution [24, 49, 50]. An example of the latter is the change of the barrier height at locations with strong curvatures, caused by the smearing out of the electronic charge [51]. Enhanced focusing can be achieved if imaging is performed with a single, rather localized electron orbital [45] such as could be provided by an adsorbate atom at the apex

of a metal tip. Lateral resolutions less than 2 Å which have been obtained on cleaved graphite [18, 43, 52] are believed to be due to such an effect. A theoretical approach especially suited to accounting for local electronic effects has recently been developed by Lang [53].

STM experiments have already provided substantial insight into the structure of reconstructed surfaces. Just as important, however, is what we have also learned about the general nature of such surfaces prepared using standard surface-preparation procedures. They are very often not as flat as generally believed or assumed. They can look quite rough, with "terraces" and flat "lakes" embedded in a hilly landscape, but, nevertheless, apparently retain their "ideal" surface structure and electronic properties—even on quite restricted flat regions [54] and in the immediate vicinity of defects [54], defect areas [12, 37], and step-lines [12, 37, 40]. This calls for necessary caution when interpreting data obtained with averaging surface analytical methods. In particular, quantitative differences in certain aspects do not indicate intrinsically different structural or electronic properties. Again, the merit of the local character of STM is obvious.

The topographical imaging capability of STM is by no means restricted to atomic-resolution levels. Imaging with a lateral resolution in the nanometer scale is certainly also accessible and of broad importance. Applications thus far include studies of thin-film growth [34, 55, 56] and technological preparation methods [57-62], new roughness standards for industrially important surfaces [63], and imaging of biological matter [62, 64, 65]. Lateral resolution at ambient pressure in the nanometer range with a vertical stability of about 1 Å is now standard with relatively simple instrumentation. Imaging is direct, without the need for decoration, staining, or replica techniques which in nanometer-scale electron microscopy provide the mass contrast or transparency required. Chemical and electronic effects can dominate topographical STM images in the angstrom range, but should be much less important in nanometer imaging [34]. Thus, the images, as obtained, are generally expected to be representative of the topographical structure being examined. Finally, adaptability to the environment is unique for imaging in both the angstrom and nanometer ranges, with fascinating prospects such as imaging of biological matter under living conditions.

A final point regarding the imaging of high-resistance materials in the constant-current mode: The potential drop in the sample, $\Delta V = IR_s$, where R_s is the spreading resistance, can vary across the surface. The applied voltage, therefore, must be larger than ΔV everywhere on the portion of the surface under examination when imaging in the constant-current mode. The relatively high voltage which was necessary in the first STM experiment on the 7×7 reconstruction of the Si(111) surface [37] could be attributed to such a spreading resistance effect [54, 66].

5. Spectroscopy and spectroscopic imaging

Tunneling spectroscopy gives access to the chemical and electronic properties of the surfaces or objects under investigation. It is concerned with density-of-state effects on the tunneling current. These effects manifest themselves in an anomalous voltage dependence of the tunneling current: they are obtained experimentally by measuring currentvoltage characteristics or derivatives thereof. In conventional tunneling spectroscopy, the tunneling barrier is a solid insulator of given width, and the applied voltage is the only external experimental parameter on which the tunneling current depends (aside, of course, from parameters such as temperature and magnetic field, which are of no concern here). In STM, however, the gap width is adjustable and its experimental control is crucial to obtaining meaningful tunneling spectra. The main merits of tunneling spectroscopy performed with an STM are the following:

- It is *local*.
- It is performed at preselected positions.
- It is performed under well-defined conditions.
- It can be combined with other methods.
- It can provide spectroscopic images.

When spectroscopy is carried out with the STM, the gap width is controlled by the tunneling current itself, either in the constant-current mode [1, 33, 67] or constant-resistance mode [68]. Therefore, the time scales of the current changes of spectroscopic interest should be either slow or fast with respect to the cutoff frequency of the tunneling-current control loop. Tunneling spectra are usually taken by superposing a small, fast modulation on the tunneling voltage while sweeping it slowly, as in conventional tunneling spectroscopy [8, 9]. Alternately, I-V curves obtained with fast voltage sweeps [31] or s-V characteristics obtained with slow sweeps [1, 67] are also used to obtain spectroscopic information. Advantages of using fast sweeps are that the shapes of the spectroscopic features which are seen are not distorted by a changing gap width and are thus more familiar in their appearance, and that STM spectroscopy can be rendered insensitive to mechanical gapwidth instabilities. An advantage of using slow sweeps is that the electric fields at the surface are prevented from becoming too high since, under the imposed condition of constant tunneling current, the gap width increases with tunneling voltage. This can be particularly important in systems with loosely bound adsorbates or delicate molecules.

Currently achievable gap-width stabilities of about 0.1 Å make it possible to carry out a large variety of spectroscopic studies, even without the necessity of very high sweep frequencies. The first examples of STM spectroscopy [1, 31, 33, 67-71] indicate good promise for the use of the STM for this purpose, even in this moderate gap-width-stability range. Many spectroscopic features can be much more pronounced

Constant-current STM image of a graphite surface: (a) raw data, (b) periodic continuation of an averaged unit cell (for the image processing method used, see [76]). The corrugation amplitude is about 1.3Å. Relative height levels of the purple, blue, green, red, and yellow regions are 0.2, 0.4, 0.73, 0.8, and 1Å, respectively, for (a), and 0.2, 0.4, 0.8, 0.9, and 1Å for (b). The solid and open circles indicate the positions of the two electronically different types of carbon atoms, which are arranged in a flat honeycomb lattice. The corrugation measured is not that of the surface carbon atoms but corresponds to that of the local density of states at the Fermi level.

in STM spectroscopy because of its local character. For instance, resonant tunneling states of the Gundlach type [72] or image states [73] are readily seen in (s vs. V) and $(\partial I/\partial V \text{ vs. } V)$ STM spectra [1, 33, 67], but only under special conditions in solid junctions. Additionally, as in inelastic tunneling spectroscopy, other aspects such as image force lowering of the tunneling barrier and reduced dielectric screening enhance spectroscopic features [74]. Finally, STM spectroscopy might relieve us, in many cases, of the necessity of observing very weak spectroscopic features. Adsorbate atoms or molecules, for instance, and their electronic states might instead be recognizable via local density-of-state effects in elastic STM tunneling spectroscopy [53] or energy dissipation [74, 75].

STS imaging should be viewed in a broad context. The scanning tunneling microscope provides images in a fivedimensional space, namely, in the three-dimensional real space (x, y, z), the tunneling current I, and the tunneling voltage V. It is the selection of the dimensions of interest which determines the "imaging mode." For the contours of constant wave-function overlap, we measure z as z(x, y) at constant I and V, and call it a "topographical" image. If we measure $(\partial I/\partial V)(x, y)$ at constant V and with I as gap-width control parameter, we obtain an STS image, and $(\partial I/\partial s)(x, y)$ gives a "work-function" profile. An STS image or a work-function profile can also be obtained from the subtraction of two topographical images taken at different voltages [32] or different currents, respectively.

One of the first STS images which was obtained pertained to the spatial variations in the superconductivity of Nb₃Sn, with the superconducting energy gap as the spectroscopic parameter of interest [31, 70]. STS of NiO [14] was mentioned above (in discussion of Figure 4). In both cases, the "topographical" images are representative of the topography, and the "spectroscopic" images of the spatial variation of the spectroscopic feature chosen. In other situations, however, we do not have such a close correspondence between image and imaging mode. The following two figures illustrate that caution is required when interpreting the topographical or electronic significance of STM and STS images.

Figure 6 shows an STM image of graphite, taken with a tunneling voltage of 50 mV [43]. The surface atomic structure of graphite is a flat, honeycomb arrangement of carbon atoms. The STM image, however, exhibits an appreciable corrugation, and two inequivalent carbon sites are found, in accord with the presence of carbon atoms having two different electronic structures. When the tunneling voltage is increased to 1.5 V, the STM image becomes flat. That obtained at V = 50 mV reflects the corrugated state density close to the Fermi level, which is very different from the integrated state density or the corrugation of the surface-atom positions. It is thus in effect a typical spectroscopic image.

Figure 7 depicts expected STM-equicurrent lines above an atomically corrugated surface. The figure provides the basis for inferring that a $\partial I/\partial V$ image of an atomically corrugated surface such as that of silicon can contain an appreciable background of structural origin. The equicurrent lines above such a corrugated but homogeneous surface are generally expected to be more closely spaced at protrusions because the corrugation amplitude of the state density decays faster than the average density itself [47], as shown in the figure.

For a tunneling current of the form $I = \varphi(V) \cdot f(V, s)$, the modulation signal is

$$\frac{\partial \ln I}{\partial V} = \left(\frac{\partial \ln \varphi}{\partial V} + \frac{\partial \ln f}{\partial V}\right). \tag{3}$$

At voltages much smaller than the effective barrier height ϕ , f is independent of V [7], and $\partial I/\partial V$ along an equicurrent line becomes independent of (x, y) even for an electrically

inhomogeneous surface described by $\varphi(V) = B(x, y)\overline{\varphi}(V)$. However, B(x, y) shows up in the equicurrent line itself, as illustrated above. In the medium-voltage range, $V \leq \phi$, we can approximate [7] $\varphi(V)$ and f(V, s) by

$$\varphi(V) = B\sqrt{\phi - V/2},$$

$$f(V, s) = \left(\frac{r+s}{s^2}\right) \cdot \exp[-(\sqrt{\phi - V/2} \cdot s)]. \tag{4}$$

Equations (4) differ from the expressions in [7] by a factor $(r+s)/\sqrt{\phi-V/2}$, which accounts for the effective area of the tunneling filament [see Equation (2), with an effective barrier height $\phi-V/2$, appropriate for the medium-voltage case]. For the ratio α of $(\partial I/\partial V)$ above a protrusion and in a valley, we obtain

$$\alpha = \frac{(s_{\rm p}\sqrt{\phi_{\rm p} - V/2} - 1)(\phi_{\rm v} - V/2)}{(s_{\rm v}\sqrt{\phi_{\rm v} - V/2} - 1)(\phi_{\rm p} - V/2)},\tag{5}$$

where the subscripts p and v refer to protrusion and valley, respectively. Since along an equicurrent line $s\sqrt{\phi - V/2} = \text{constant} >> 1$ (up to corrections in $\ln s$ and $\ln \phi$ which are of the order of 1), a good approximation for (5) is

$$\alpha = \frac{\phi_{\rm v} - V/2}{\phi_{\rm p} - V/2} \approx \left(\frac{s_{\rm p}}{s_{\rm v}}\right)^2 < 1. \tag{6}$$

Thus, $\partial I/\partial V|_{I}$ contains a background of structural origin which appears qualitatively as inverted topography. In the field-emission range, $V > \phi$, the spectroscopic image again becomes structureless, as was the case at very low voltages.

Figure 8 illustrates the similarity of the strong, structural background of an STS image to associated surface topography. The general correspondence is clearly visible. The dominant true spectroscopic features are the three pronounced maxima in the upper half of each unit cell. corresponding to the three weakest minima in the STM images (denoted by the white circles). These, as well as other noticeable differences between the upper and lower halves of the 7×7 unit cell [37, 38, 42, 54, 71], are not observed for a positive voltage [54]. The disturbance in the region of the triangle of Figures 8(c) and (d) extends over a larger area in the STS image than in the STM image. Detailed spectroscopic information is thus not readily available from a single STS image [77]. On the other hand, the structural background facilitates the locating of pronounced spectroscopic features. Figure 9 shows the topographical and spectroscopic images of the 7×7 reconstruction of the Si(111) surface after exposure for several hours to a residual pressure of 10⁻⁸ Pa. The images were obtained shortly before the adsorption from the residual gas had quenched the 7×7 reconstruction. Appreciable disorder is already evident in the images. There is experimental evidence that adsorption occurs on distinct sites of the 7×7 surface unit cell [78]. A small structure is observed in the topographical image near the center minimum [37, 54] of the lower half of the

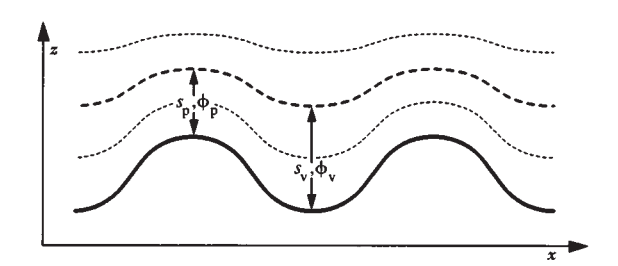


Figure 7

Expected STM-equicurrent lines (dashed lines) above an atomically corrugated surface (solid line). The different spacings of the equicurrent lines at the protrusions and in the valleys can be described by a varying effective tunneling barrier height.

 7×7 unit cell of Figure 8; the structure is absent in a freshly prepared surface. It appears, depending on the resolution which is achieved, as a small maximum or terrace, displaced slightly from the center of the minimum. In the $\partial I/\partial V$ image, pronounced peaks appear at the same positions, superimposed on the structural background. Although we cannot yet associate this spectroscopic feature with a distinct electronic structure, it appears reasonable to relate it to the adsorption site. Furthermore, we have found that the 7×7 cell can accommodate a second adsorbate after all of the center minima have become occupied. The second site is one of the edge minima [37, 54]. It can vary from experiment to experiment or region to region, but once a second site has accommodated an adsorbate, only equivalent sites are further occupied. The structure becomes disordered after the latter have become occupied.

6. Other types of imaging

Other types of STM imaging which have been achieved thus far include the imaging of work-function profiles [79, 80], potential distributions [29, 81], and dynamic events or transients [82, 83]. The local work function or, correctly speaking, the effective tunneling barrier height can be derived from I(s) at constant V[1, 5, 19] or from s(V) at constant I[74, 84]. Work-function profiles, in practice, are obtained by modulating the distance at high frequencies while controlling the average gap width by means of the STM mode. The modulation signal divided by the current is, neglecting logarithmic terms in s,

$$-\partial(\ln I)/\partial s = \sqrt{\phi} + (1/2\sqrt{\phi}) \cdot \partial \phi/\partial s. \tag{7}$$

We should like to stress at this point that the expression "work-function profile" is misleading in the sense that the effective barrier height ϕ obtained from (7) generally differs from the work function. The effective barrier is some average

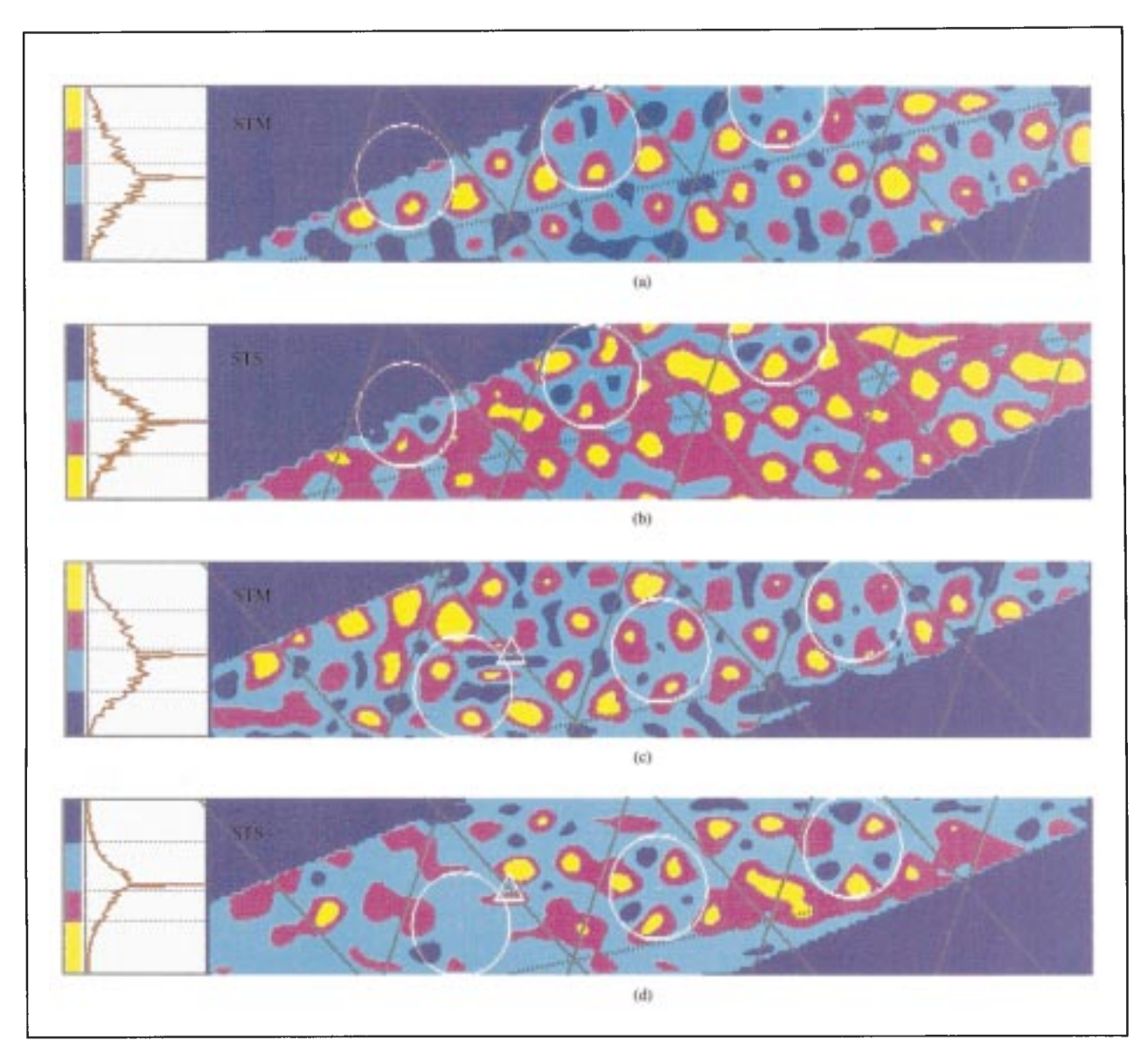


Figure 8 STM and STS images of the 7×7 reconstructed Si(111) surface, taken with tip at -0.8 V for STM image (a) and STS image (b) and at -1.0 V for STM image (c) and STS image (d). Note the inverted color sequence of the STS images. The rhomboidal 7×7 unit cells are indicated by the solid and (central) dashed lines. Specific features discussed in the text are located within the white circles. A local disturbance in the region of the triangle in (c) and (d) is associated with a missing adatom at the upper right portion of that triangle.

over the actual barrier height across the gap. The work function is equal to this actual height only at infinite distance from the surface, i.e., at distances s where the second term in (7) becomes negligible. And it is an average of the actual potential barrier over distances parallel to the surface larger than s. Thus, by definition, work-function profiles cannot exhibit structure on a small lateral scale. The barrier height, on the other hand, is a local electronic

property and is closely related to the local electronic charge; e.g., the barrier is enhanced if excess electronic charge is present and lowered if there is a charge deficiency. For a gap-width-independent ϕ , the second term on the right-hand side of (7) is zero, and the s modulation signal is a direct measure of the local ϕ . In practice, however, ϕ depends on s, in particular at the small gap widths present in an STM. The two major sources for this s-dependence are local charge

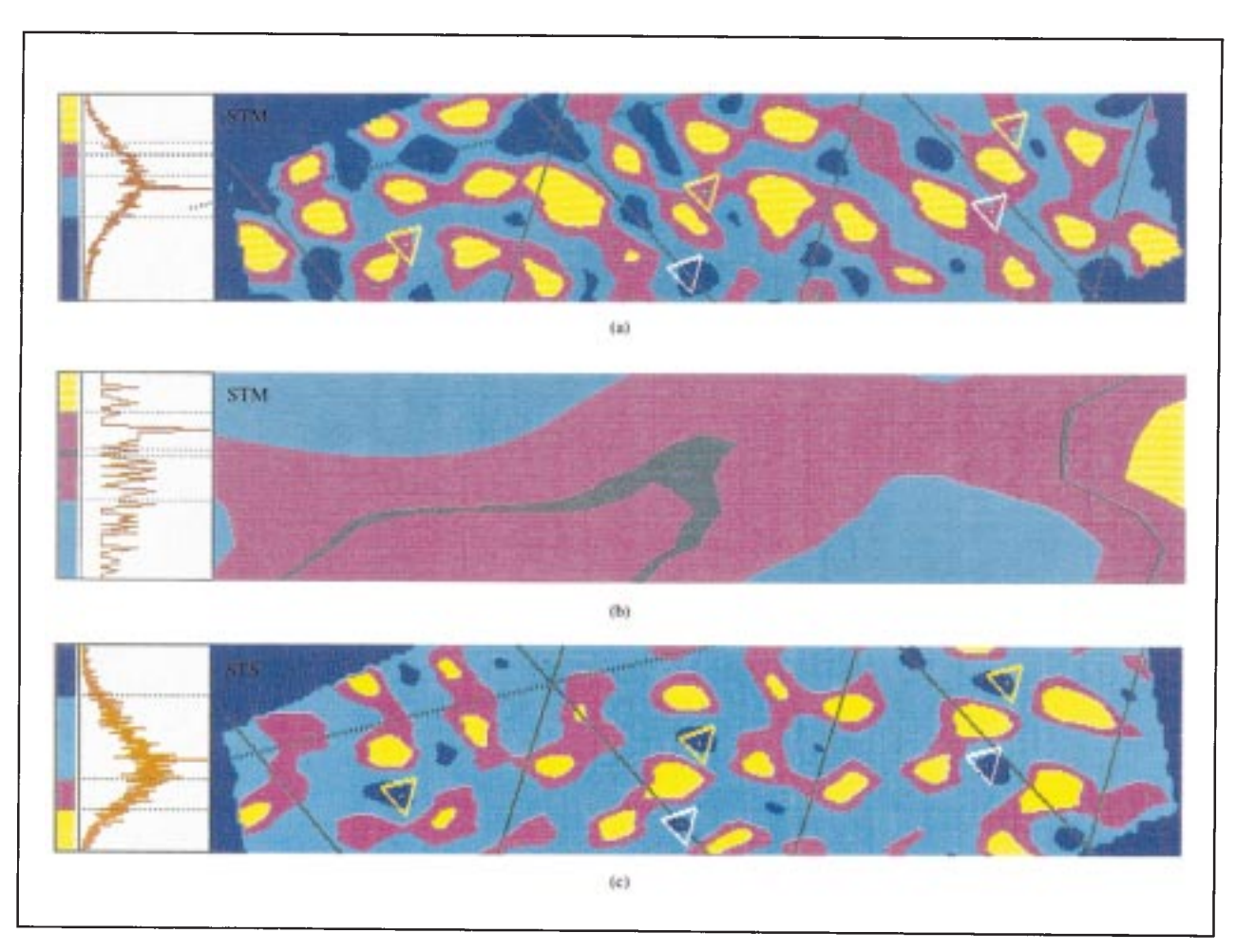


Figure 9

(a) STM image, (b) enlarged portion of the region in (a) in the vicinity of central yellow triangle, and (c) STS image of the 7×7 reconstructed Si(111) surface in the presence of two adsorbates per surface unit cell. Center and edge adsorbate in (a) and (c) are indicated, respectively, by yellow and white triangles. The adsorbate position in the central yellow triangle is identified as the widened portion of the dark ribbon which appears at a relative height between 0.70 and 0.72 in (a) and (b). Other adsorbate positions become visible at slightly different heights.

variations and the image potential [73]. The former are an intrinsic property of the local surface chemistry or electronic structure, the latter a general aspect of an electron moving to or from the surface. Fortunately, the image-potential influence on $\partial \ln I/\partial s$ is not very large and practically independent of s for s > 4 Å [49]. This is an interesting result in view of the substantial reduction of the tunneling-barrier height by the image potential at such distances, e.g., by a factor of four at 4 Å. The image potential only slightly reduces the measured values of $\partial \ln I/\partial s$, but does not induce any structure.

Another point concerns the method itself. Distances are monitored or controlled in the z-direction, i.e., perpendicular to the average surface. The gap width s, on the other hand, is a distance in the direction of the tunneling-

current filament, which is roughly perpendicular to the *local* surface element. The measured values of $\partial I/\partial z$ thus depend on the local geometry, and "barrier-height images" contain topographical features. In analogy with spectroscopic imaging, a uniform barrier height does not result in a structureless $\partial I/\partial z$ image. Since $\partial I/\partial s = (\partial I/\partial z)/\sin\Theta$, where Θ is the angle between z and the local surface gradient, the measured modulation signal underestimates ϕ .

Our final point concerns the magnitude of the experimentally determined values of ϕ . Very often, they are considerably smaller than expected and only on clean and flat surfaces do they approach those of the work function. A reduction of, say, 50% can reasonably be attributed to image potential and corrugation effects [50]; however, values observed in the tenths-of-eV range for vacuum gaps have so

far remained unexplained. Questions relating to reduced barrier heights are addressed in more detail in the papers by Garcia [50] and Coombs and Pethica [85].

In scanning potentiometry, the local electric potential along the surface is imaged. The tunneling tip serves as a local potential probe in a bridge-type arrangement. It is expected that this may become a very useful method in the electrical testing of very small structures. A possible configuration has been worked out and implemented by Muralt, Pohl, and Denk [29] and by Muralt and Pohl [81].

In transient imaging, current changes as a function of time are considered. In one type of experiment, the transients are induced by species diffusing through the tunneling region [82]. They appear as tunneling-current spikes of distinct shape or, if slow or strong enough, as spikes of similar shape in the topographical image. Besides the possibility of observing individual diffusion processes, the direct correlation of diffusion with particular surface features will make this a very interesting method for surface-diffusion studies [86]. In another type of experiment [83], transients are used to identify electron trapping sites. Tunneling electrons trapped on or immediately below the surface give rise to a type of Coulomb blocking by temporarily increasing the effective barrier height for other electrons.

7. Local displacement monitoring and control

A first example of such use of an STM reported in the literature is that of position control of the detector of an optical stethoscope [87]. This instrument is capable of optical imaging far below the diffraction limit, while functioning as an STM. More recently, Binnig, Quate, and Gerber [88(a)] introduced a far-reaching application of the STM for measurements of ultrasmall forces. The method requires measuring small displacements of a soft cantilevertype spring. In order to render the force detector insensitive to vibrations, its mechanical eigenfrequency must be high; viz., a very light and small cantilever is required. By using vacuum tunneling to monitor displacements of such small cantilevers, force measurements down to the 10⁻¹⁸ N range are envisaged. The first realization of this concept is the Atomic Force Microscope (AFM) [88(a)]. The forces to be measured are the interatomic forces between the surface atoms under investigation and the apex atoms of a very sharp diamond tip fixed on the conducting cantilever. Bending of the cantilever by the interatomic forces is monitored by the tunneling current between the cantilever and an STM tip. Scanning the diamond tip across the conducting or insulating surface under investigation (or, in the above version of the AFM, moving the surface across the tip) at constant interatomic force yields a topographical image of the surface. The AFM image is composed of contours of constant force between the imaged surface and a probe tip, in close analogy with that obtained using Stylus Profilometry [13]. However, the forces used in the AFM are

in the 10⁻¹⁰ N range or smaller compared to typical stylus loads of 10⁻³ N, and the AFM imaging process can be considered as nondestructive. Recently, the role of forces acting in scanning tunneling microscopy has been discussed in more detail [88(b), (c)]. Soler et al. [88(b)] have shown that elastic deformations induced by interatomic forces between tip and surface are the primary cause of the giant corrugations observed in graphite [43] and laminar compounds [39]. Dürig et al. [88(c)] present experimental evidence for the forces acting in STM by imaging surfaces on a soft cantilever beam. These two investigations open new prospects in STM.

8. Local modifications and processing

An important aspect of the applications discussed thus far has been the nondestructive use of the tunneling-current filament and tip. Alternatively, the opposite can be done; viz., intentionally induce *local changes*. The tip then serves both as a local processing tool and as a probe for imaging the changes. Depending on how the tip is used, processing might be of a mechanical, electrical, thermal, or chemical nature.

Mechanical deformations produced and imaged by an STM tip have been reported by Abraham et al. [89] and by van Kempen and van de Walle [90]. In the latter work, indentations were made which were some hundred Å deep. After each contact, the indentations were imaged with the tip and were found to be reproducible and pyramid-like, with relatively sharp edges—an interesting finding in its own right, and an example of the use of an STM tip for relatively rough mechanical treatment of a surface.

Processes which are electrically induced, whether via the tunneling electron beam or via the high electric fields associated with it, are aimed at both structural and chemical modifications. They are envisaged as potentially useful for nanomachining, material deposition and removal, chemical and lithographic processing, etc. Two efforts reported thus far pertain to inducing chemical modifications [91, 92].

9. Concluding remarks

Scanning tunneling microscopy is on its way to becoming a viable method for real-space imaging of structural, chemical, and electronic properties of surfaces. Its adaptability to various environments and utilization of relatively low electron energies make it potentially attractive as a microscopic technique for use in diverse areas in science and technology; its applications in local probing and specimen modification on an atomic scale open exciting possibilities beyond imaging.

Acknowledgment

We should like to take this opportunity to thank all of our colleagues who have contributed their efforts over the years, with suggestions regarding the technical development of the STM, assistance in experiments and data and image processing, and guidance in connection with theoretical aspects. We also want to express our appreciation of the continuing support by the members of the Central Scientific Services Department of our Laboratory. And our thanks are due to the IBM Europe Institute for sponsoring a most stimulating workshop on this subject.

References and notes

- G. Binnig and H. Rohrer, "Scanning Tunneling Microscopy," Helv. Phys. Acta 55, 726 (1982).
- R. H. Fowler and L. Nordheim, "Electron Emission in Intense Electric Fields," Proc. Roy. Soc. Lond. A 119, 173 (1928); J. Frenkel, "On the Electrical Resistance of Contacts Between Solid Conductors," Phys. Rev. 36, 1604 (1930).
- L. Esaki, "New Phenomenon in Narrow Germanium p-n Junctions," Phys. Rev. 109, 603 (1958); I. Giaever, "Energy Gap in Superconductors Measured by Electron Tunneling," Phys. Rev. Lett. 5, 147 (1960).
- I. Giaever, "Electron Tunneling and Superconductivity," Rev. Mod. Phys. 46, 245 (1974).
- 5. R. Young, J. Ward, and F. Scire, "The Topografiner: An Instrument for Measuring Surface Microtopography," Rev. Sci. Instrum. 43, 999 (1972); W. A. Thompson and S. F. Hanrahan, "Thermal Drive Apparatus for Direct Vacuum Tunneling Experiments," Rev. Sci. Instrum. 47, 1303 (1976); E. C. Teague, "Room Temperature Gold-Vacuum-Gold Tunneling Experiments," Bull. Amer. Phys. Soc. 23, 290 (1978); U. Poppe, "Tunneling Experiments on a Single Crystal of E_rRh₄B₄," Physica B & C 108, 805 (1981); for references on the GaAs probe tunneling method see G. Güntherodt, W. A. Thompson, and F. Holtzberg, "Electron Tunneling into Intermediate-Valence Materials," Phys. Rev. Lett. 49, 1030 (1982).
- The workshop was held in Oberlech, Austria, under the auspices of the IBM Europe Institute, July 1-5, 1985.
- J. Simmons, "Generalized Formula for the Electric Tunnel Effect Between Similar Electrodes Separated by a Thin Insulating Film," J. Appl. Phys. 34, 1793 (1963).
- See, e.g., C. B. Duke, "Tunneling in Solids," Academic Press, Inc., New York, 1969; E. L. Wolf, "Electron Tunneling Spectroscopy," Rep. Prog. Phys. 41, 1439 (1978).
- R. C. Jaklevic and J. Lambe, "Molecular Vibration Spectra by Electron Tunneling," Phys. Rev. Lett. 17, 1139 (1966); idem, Tunneling Spectroscopy: Capabilities, Applications, and New Techniques, P. Hansma, Ed., Plenum Press, New York, 1982.
- J. Bardeen, "Tunneling from a Many-Particle Point of View," Phys. Rev. Lett. 6, 57 (1961).
- E. Stoll, A. Baratoff, A. Selloni, and P. Carnevali, "Current Distribution in the Scanning Vacuum Tunneling Microscope: A Free Electron Model," J. Phys. C 17, 3073 (1984).
- G. Binnig, H. Rohrer, Ch. Gerber, and E. Stoll, "Real-Space Observation of the Reconstruction of Au(100)," Surf. Sci. 144, 321 (1984).
- J. B. P. Williamson, "Microphotography of Surfaces," Proc. Inst. Mech. Eng. London 182, 21 (1967-68); see also the American National Standard Surface Texture, ANSI B46.1 (1978 Edition).
- 14. G. Binnig, H. Fuchs, J. Kübler, F. Salvan, and A. R. Williams, "Scanning Tunneling Microscope Spectroscopy and the Low-Energy Excitation Spectrum of NiO," unpublished work; R. Garcia, J. J. Saenz, and N. Garcia, "Conductivity and Structure of Thin Oxide Layers Grown on a Metal Substrate: Scanning Tunneling Microscopy in NiO on Ni(100)," *Phys. Rev. B* 33, 4439 (1986).
- H. H. Farrell and M. Levinson, "Scanning Tunneling Microscope as a Structure Modifying Tool," *Phys. Rev. B* 31, 3593 (1985).
- Dieter W. Pohl, "Some Design Criteria in Scanning Tunneling Microscopy," *IBM J. Res. Develop.* 30, pp. 417–427 (1986, this issue).

- Hans-Werner Fink, "Mono-Atomic Tips for Scanning Tunneling Microscopy," *IBM J. Res. Develop*. (to be published in Sept. 1986).
- Sang-Il Park and C. F. Quate, "Tunneling Microscopy of Graphite in Air," Appl. Phys. Lett. 48, 112 (1986); A. Bryant, D. P. E. Smith, and C. F. Quate, "Imaging in Real Time with the Tunneling Microscope," Appl. Phys. Lett. 48, 832 (1986).
- G. Binnig, H. Rohrer, Ch. Gerber, and E. Weibel, "Vacuum Tunneling," *Physica* 109 & 110B, 2075 (1982); *idem*, "Tunneling Through a Controllable Vacuum Gap," *Appl. Phys. Lett.* 40, 178 (1982).
- G. Binnig and H. Rohrer, "The Scanning Tunneling Microscope," Sci. Amer. 253, 50 (1985).
- Ch. Gerber, G. Binnig, H. Fuchs, O. Marti, and H. Rohrer, "Scanning Tunneling Microscope Combined with a Scanning Electron Microscope," Rev. Sci. Instrum. 57, 221 (1986).
- D. P. E. Smith and S. A. Elrod, "Magnetically Driven Micropositioners," Rev. Sci. Instrum. 56, 1970 (1985).
- M. Ringger, B. W. Corb, H. R. Hidber, R. Schlögl, R. Wiesendanger, A. Stemmer, L. Rosenthaler, A. J. Brunner, P. Oelhafen, and H.-J. Güntherodt, "STM Activity at the University of Basel," *IBM J. Res. Develop*. (to be published in Sept. 1986).
- 24. Roy F. Willis, M. C. Payne, J. B. Payne, M. D. Pashley, and J. H. Coombs, "Vacuum Tunneling Microscopy—A Status Report," Festkörper Probleme XXV, p. 699, P. Grosse, Ed., Friedr. Vieweg & Sohn, Braunschweig/Wiesbaden, Federal Republic of Germany, 1985.
- J. Moreland, S. Alexander, M. Cox, R. Sonnenfeld, and P. Hansma, "Squeezable Electron Tunnel Junctions," Appl. Phys. Lett. 43, 387 (1983); J. Moreland and P. K. Hansma, "Electromagnetic Squeezer for Compressing Squeezable Electron Tunnel Junctions," Rev. Sci. Instrum. 55, 399 (1984); P. K. Hansma, "Squeezable Tunneling Junctions," IBM J. Res. Develop. 30, pp. 370-373 (1986, this issue).
- J. E. Demuth, R. J. Hamers, R. M. Tromp, and M. E. Welland, "A Scanning Tunneling Microscope for Surface Science Studies," *IBM J. Res. Develop.* 30, pp. 396–402 (1986, this issue); *idem*, "A Simplified Scanning Tunneling Microscope for Surface Science Studies," *J. Vac. Sci. Technol. A*, accepted for publication.
- B. Drake, R. Sonnenfeld, J. Schneir, P. K. Hansma, G. Slough, and R. V. Coleman, "A Tunneling Microscope for Operation in Air and Fluids," Rev. Sci. Instrum. 57, 441 (1986).
- G. F. A. van de Walle, J. W. Gerritsen, H. van Kempen, and P. Wyder, "High-Stability Tunneling Microscope," Rev. Sci. Instrum. 56, 1573 (1985).
- P. Muralt, D. W. Pohl, and W. Denk, "Wide-Range, Low-Operating-Voltage, Bimorph STM: Application as Potentiometer," *IBM J. Res. Develop.* (to be published in Sept. 1986).
- G. Binnig and H. Rohrer, "Scanning Tunneling Microscopy," Surf. Sci. 126, 236 (1983).
- A. L. de Lozanne, S. A. Elrod, and C. F. Quate, "Spatial Variation in the Superconductivity of Nb₃Sn Measured by Low-Temperature Tunneling Microscopy," *Phys. Rev. Lett.* 54, 2433 (1985).
- R. M. Feenstra and A. P. Fein, "Scanning Tunneling Microscopy of Cleaved Semiconductor Surfaces," *IBM J. Res. Develop.* (to be published in Sept. 1986).
- R. S. Becker, J. Golovchenko, and B. S. Swartzentruber, "Electron Interferometry at Crystal Surfaces," *Phys. Rev. Lett.* 55, 987 (1985).
- J. K. Gimzewski, A. Humbert, J. G. Bednorz, and B. Reihl, "Silver Films Condensed at 300 and 90 K: Scanning Tunneling Microscopy of Their Surface Topography," *Phys. Rev. Lett.* 55, 951 (1985).
- H. R. Ott, Institute for Solid State Physics, ETH, Zurich, Switzerland, and H. Rohrer, unpublished work.
- S. Vieira, "Behavior and Calibration of Some Piezoelectric Ceramics Used in the Scanning Tunneling Microscope," *IBM J. Res. Develop.* (to be published in Sept. 1986).

- 37. G. Binnig, H. Rohrer, Ch. Gerber, and E. Weibel, "7 × 7 Reconstruction on Si(111) Resolved in Real Space," Phys. Rev. Lett. 50, 120 (1983); idem, "(111) Facets as the Origin of Reconstructed Au(110) Surfaces," Surf. Sci. 131, L379 (1983); A. M. Baro, G. Binnig, H. Rohrer, Ch. Gerber, E. Stoll, A. Baratoff, and F. Salvan, "Real-Space Observation of the 2×1 Structure of Chemisorbed Oxygen on Ni(110) by Scanning Tunneling Microscopy," Phys. Rev. Lett. 52, 1304 (1984).
- 38. R. S. Becker, J. A. Golovchenko, and B. S. Swartzentruber, 'Tunneling Images of Germanium Surface Reconstructions and Phase Boundaries," Phys. Rev. Lett. 54, 2678 (1985); idem, "Tunneling Images of the 5 × 5 Surface Reconstruction on Ge-Si(111)," Phys. Rev. B 32, 8455 (1985); R. S. Becker, J. A. Golovchenko, E. G. McRae, and B. Swartzentruber, "Tunneling Images of Atomic Steps on the Si(111) 7×7 Surface," Phys. Rev. Lett. 55, 2028 (1985).
- 39. R. V. Coleman, B. Drake, P. K. Hansma, and G. Slough, "Charge-Density Waves Observed with a Tunneling Microscope," Phys. Rev. Lett. 55, 394 (1985).
- 40. R. J. Behm, W. Hoesler, E. Ritter, and G. Binnig, "Correlation Between Domain Boundaries and Surface Steps-An STM Study on Reconstructed Pt(100)," Phys. Rev. Lett. 56, 228 (1986); W. Hösler, R. J. Behm, and E. Ritter, "Defects on the Pt(100) Surface and Their Influence on Surface Reactions-Scanning Tunneling Microscopy Study," IBM J. Res. Develop. 30, pp. 403-410 (1986, this issue).
- 41. R. M. Feenstra and A. P. Fein, "Surface Morphology of GaAs(110) by Scanning Tunneling Morphology," Phys. Rev. B 32, 1394 (1985); R. M. Feenstra, W. A. Thompson, and A. P. Fein, "Real-Space Observation of π Bonded Chains and Surface Disorder on Si(111) 2 × 1," Phys. Rev. Lett. 56, 608 (1986); R. M. Feenstra, W. A. Thompson, and A. P. Fein, "Scanning Tunneling Microscopy Studies of Si(111) 2×1 Surfaces, J. Vac. Sci. Technol. All 4 (May/June 1986).
- 42. R. M. Tromp, R. J. Hamers, and J. E. Demuth, "Si(100) Dimer Structure Observed with Scanning Tunneling Microscopy,' Phys. Rev. Lett. 55, 1303 (1985); R. J. Hamers, R. M. Tromp, and J. E. Demuth, "Scanning Tunneling Microscopy of Si(100)," unpublished work; idem, "Atomic and Electronic Contributions to Si(111) (7×7) Scanning Tunneling Microscopy Images," Phys. Rev. B, accepted for publication.
- 43. G. Binnig, H. Fuchs, Ch. Gerber, H. Rohrer, E. Stoll, and E. Tosatti, "Energy-Dependent State-Density Corrugation of a Graphite Surface as Seen by Scanning Tunneling Microscopy," Europhys. Lett. 1, 31 (1986).
- 44. J. Tersoff and D. R. Hamann, "Theory and Application for the Scanning Tunneling Microscope," Phys. Rev. Lett. 50, 1998 (1983); J. Tersoff and D. R. Hamann, "Theory of the Scanning Tunneling Microscope," Phys. Rev. B 31, 805 (1985).
- 45. A. Baratoff, "Theory of Scanning Tunneling Microscopy (STM)," Europhys. Conf. Abstr. 7B, 364 (1983).
- 46. N. Garcia, C. Ocal, and F. Flores, "Model Theory for Scanning Tunneling Microscopy: Application to Au(110) (1 \times 2)," Phys. Rev. Lett. 50, 2002 (1983); N. Garcia and F. Flores, "Theoretical Studies for Scanning Tunneling Microscopy," Physica 127B, 137 (1984).
- 47. A. Baratoff, "Theory of Scanning Tunneling Microscopy-Methods and Approximations," Physica 127B, 143 (1984).
- 48. E. Stoll, "Resolution of the Scanning Tunneling Microscope," Surf. Sci. 143, L411 (1984).
- 49. G. Binnig, N. Garcia, H. Rohrer, J. M. Soler, and F. Flores, "Electron-Metal-Surface Interaction Potential with Vacuum Tunneling: Observation of the Image Force," Phys. Rev. B 30, 4816 (1984).
- 50. N. Garcia, "Theory of Scanning Tunneling Microscopy and Spectroscopy: Resolution, Image, and Field States and Thin Oxide Layers," IBM J. Res. Develop. (to be published in Sept. 1986).
- 51. R. Smoluchowski, "Anisotropy of the Electronic Work Function of Metals," Phys. Rev. 60, 661 (1941); N. D. Lang, "Density Functional Formalism and the Electronic Structure of Metal Surfaces," Solid State Phys. 28, 225 (1973).

- 52. Cleaved pyrolithic graphite appears to become the ideal "test surface" for STM. A lateral resolution under 2 Å is readily achievable in vacuum and air (J. Gimzewski, H. Güntherodt, A. Humbert, and H. Salemink, private communications) and even under water [R. Sonnenfeld and P. K. Hansma, "Atomic Resolution Microscopy in Water," Science 232, 211 (April 11, 1986).] The crucial role of the electronic surface structure itself in obtaining such high resolution on special surfaces such as that of graphite is pointed out by J. Tersoff, "Anomalous Corrugation in Scanning Tunneling Microscopy of Low-Dimensionality Semiconductors and Semimetals," Phys. Rev. Lett. 56 (1986).
- 53. N. Lang, "Vacuum Tunneling Current from an Adsorbed Atom," Phys. Rev. Lett. 55, 230 (1985); idem, "Electronic Structure and Tunneling Current for Chemisorbed Atoms, IBM J. Res. Develop. 30, pp. 374-379 (1986, this issue); idem, "Theory of Single Atom Imaging in the Scanning Tunneling Microscope," Phys. Rev. Lett. 56, 1164 (1986).
- 54. G. Binnig, H. Rohrer, F. Salvan, Ch. Gerber, and A. M. Baró, "Revisiting the 7×7 Reconstruction of Si(111)," Surf. Sci. 157, L373 (1985).
- 55. A. Humbert, J. K. Gimzewski, and B. Reihl, "Post-Annealing of Coldly Condensed Ag Films: Influence of Pyridine Preadsorption," Phys. Rev. B 32, 4252 (1985).
- 56. Th. Berghaus, H. Neddermeyer, and St. Tosch, "A Scanning Tunneling Microscope for the Investigation of the Growth of Metal Films on Semiconductor Surfaces," IBM J. Res. Develop. (to be published in Sept. 1986).
- 57. R. Miranda, N. Garcia, A. M. Baró, R. Garcia, J. L. Pena, and H. Rohrer, "Technological Applications of Scanning Tunneling Microscopy at Atmospheric Pressure," Appl. Phys. Lett. 47, 367
- 58. S. Chiang and R. J. Wilson, "Scanning Tunneling Microscopy," Improved Methods for Examining the Submicron World, Plenum Press (to be published in 1986); idem, "Construction of a UHV Scanning Tunneling Microscope," IBM J. Res. Develop. (to be published in Sept. 1986).
- 59. R. M. Feenstra and G. S. Oehrlein, "Surface Morphology of Oxidized and Ion-Etched Silicon by Scanning Tunneling Microscopy," J. Vac. Sci. Technol. B 3, 1136 (1985); idem, Appl. Phys. Lett. 47, 97 (1985).
- 60. J. K. Gimzewski, A. Humbert, D. W. Pohl, and S. Vepřek, "Scanning Tunneling Microscopy of Nanocrystalline Silicon Surfaces," Surf. Sci. 168, 795 (1986).
- M. Ringger, H. R. Hidber, R. Schlögl, P. Oelhafen, H.-J. Güntherodt, K. Wandelt, and G. Ertl, "Vacuum Tunneling Applied to the Surface Topography of a Pd(100) Surface,' Proceedings of the 17th International Conference on Low Temperature Physics LT-17, 25 (1984), North-Holland, Amsterdam.
- 62. A. M. Baró, R. Miranda, and J. L. Carrascosa, "Application to Biology and Technology of the Scanning Tunneling Microscope Operated in Air at Ambient Pressure," IBM J. Res. Develop. 30, pp. 380-386 (1986, this issue).
- 63. N. Garcia, A. M. Baró, R. Miranda, H. Rohrer, Ch. Gerber, R. Garcia Cantu, and J. L. Pena, "Surface Roughness Standards, Obtained with the Scanning Tunneling Microscope Operated at Atmospheric Air Pressure," *Metrologia* 21, 135 (1985).
 64. G. Binnig and H. Rohrer, "Scanning Tunneling Microscopy,"
- Trends in Physics 1984, J. Janta and J. Pantoflicek, Eds., European Physical Society, 1985, pp. 38-46.
- 65. A. M. Baró, R. Miranda, J. Alaman, N. Garcia, G. Binnig, H. Rohrer, Ch. Gerber, and J. L. Carrascosa, "Determination of Surface Topography of Biological Specimens at High Resolution by Scanning Tunneling Microscopy," Nature 315, 253 (1985).
- 66. F. Flores and N. Garcia, "Voltage Drop in the Experiments of Scanning Tunneling Microscopy for Si," Phys. Rev. B 30, 2289 (1984).
- 67. G. Binnig, K. H. Frank, H. Fuchs, N. Garcia, B. Reihl, H. Rohrer, F. Salvan, and A. R. Williams, "Tunneling Spectroscopy and Inverse Photoemission: Image and Field States," Phys. Rev. Lett. 55, 991 (1985).

- 68. W. J. Kaiser and R. C. Jaklevic, "Scanning Tunneling Microscopy of Surfaces," Bull. Amer. Phys. Soc. 30, 309 (1985); idem, "Spectroscopy of Electronic States of Metals with a Scanning Tunneling Microscope," IBM J. Res. Develop. 30, pp. 410-416 (1986, this issue).
- A. Baratoff, G. Binnig, H. Fuchs, F. Salvan, and E. Stoll, "Tunneling Microscopy and Spectroscopy of Semiconductor Surfaces and Interfaces," Surf. Sci. 168, 734 (1986).
- S. A. Elrod, A. Bryant, A. L. de Lozanne, S. Park, D. Smith, and C. F. Quate, "Tunneling Microscopy from 300 to 4.2 K," *IBM* J. Res. Develop. 30, pp. 387-395 (1986, this issue).
- R. S. Becker, J. A. Golovchenko, D. R. Hamann, and B. S. Swartzentruber, "Real-Space Observation of Surface States on Si(111) 7 × 7 with the Tunneling Microscope," *Phys. Rev. Lett.* 55, 2032 (1985).
- K. H. Gundlach, "Zur Berechnung des Tunnelstromes durch eine Trapezformige Potentialstufe," Solid-State Electron. 9, 949 (1966).
- 73. N. Garcia and J. Solana, "Surface States in a One-Dimensional Crystal," Surf. Sci. 36, 262 (1973); P. M. Echenique and J. B. Pendry, "The Existence and Detection of Rydberg States at Surfaces," J. Phys. C 11, 2056 (1978); for further references see N. Garcia, B. Reihl, K. H. Frank, and A. R. Williams, "Image States: Binding Energies, Effective Masses, and Surface Corrugation," Phys. Rev. Lett. 54, 591 (1985).
- G. Binnig, N. Garcia, and H. Rohrer, "Conductivity Sensitivity of Inelastic Scanning Tunneling Microscopy," *Phys. Rev. B* 32, 1336 (1985).
- 75. B. N. J. Persson and J. E. Demuth, "Inelastic Electron Tunneling from a Metal Tip," Solid State Commun. 57, 769 (1986). F. Flores, P. M. Echenique, and R. H. Ritchie, "Energy Dissipation Processes in the Scanning Tunneling Microscopy," Universidad Autónoma de Madrid, unpublished work.
- E. Stoll, "Information- and Image-Processing of Scanning Tunneling Microscope Data," Proceedings of the 2nd International Technical Symposium on Optical and Electro-Optical Applied Science and Engineering, Cannes, Dec. 2-6, 1985, in press.
- A. Baratoff, G. Binnig, H. Fuchs, H. Rohrer, E. Stoll, and F. Salvan, "Interpretation of Scanning Tunneling Spectroscopic (STS) Images—Applications to 7 × 7 Si(111)," Europhys. Conf. Abstr. 10B, 0-31 (1986); idem, Surf. Sci. (accepted for publication); R. J. Hamers, R. M. Tromp, and J. E. Demuth, "Surface Electronic Structure of Si(111) 7 × 7 Resolved in Real Space," Phys. Rev. Lett. 56 (1986).
- E. Conrad and M. B. Webb, "Xe and Kr Adsorption on the Si(111) 7 × 7 Surface," Surf. Sci. 129, 37 (1983); J. E. Demuth and A. J. Schell-Sorokin, "Rare Gas Titration Studies of Si(111) Surfaces," J. Vac. Sci. Technol. A2, 808 (1983).
- G. Binnig and H. Rohrer, "Scanning Tunneling Microscopy," Surf. Sci. 126, 236 (1983).
- M. S. Khaikin and A. M. Trojanovsky, "A Scanning Tunneling Microscope with a Modulated Tunneling Gap Operating in a Liquid Medium," Pis'ma Zh. Tech. Phys. 11, 1236 (1985).
- 81. P. Muralt and D. W. Pohl, "Scanning Tunneling Potentiometry," Appl. Phys. Lett. 48, 514 (1986).
- G. Binnig, H. Fuchs, and E. Stoll, "Surface Diffusion of Oxygen Atoms Individually Observed by STM," Surf. Sci. (1986, in press).
- M. E. Welland and R. H. Koch, "Spatial Location of Electron Trapping Defects on Silicon by Scanning Tunneling Microscopy," *Appl. Phys. Lett.* 48, 724 (1986).
- M. D. Pashley, J. B. Pethica, and J. Coombs, "Scanning Tunneling Microscope Studies," Surf. Sci. 152/153, 27 (1985).
- J. H. Coombs and J. B. Pethica, "Properties of Vacuum Tunneling Currents: Anomalous Barrier Heights," *IBM J. Res. Develop.* (to be published in Sept. 1986).
- R. Gomer, "Extensions of the Field Emission Fluctuation Method for the Determination of Surface Diffusion Coefficients," J. Appl. Phys. A39, 1 (1986).
- D. W. Pohl, W. Denk, and M. Lanz, "Optical Stethoscopy: Image Recording with Resolution λ/20," Appl. Phys. Lett. 44,

- 651 (1984); U. Dürig, D. W. Pohl, and F. Rohner, "Near-Field Optical Scanning Microscopy," *J. Appl. Phys.* **59** (1986); *idem*, "Near-Field Optical Scanning Microscopy with Tunnel-Distance Regulation," *IBM J. Res. Develop.* (to be published in Sept. 1986).
- 88. (a) G. Binnig, C. F. Quate, and Ch. Gerber, "The Atomic Force Microscope," *Phys. Rev. Lett.* 56, 930 (1986); (b) J. M. Soler, A. M. Baró, N. Garcia, and H. Rohrer, "Interatomic Forces in Scanning Tunneling Microscopy: Giant Corrugations of the Graphite Surface," unpublished work; (c) U. Dürig, J. Gimzewski, and D. W. Pohl, "Experimental Observations of Forces Acting During Scanning Tunneling Microscopy," unpublished work.
- David W. Abraham, H. Jonathon Mamin, Eric Ganz, and John Clarke, "Surface Modification with the Scanning Tunneling Microscope," *IBM J. Res. Develop.* (to be published in Sept. 1986).
- 90. H. van Kempen and G. F. A. van de Walle, "Applications of a High-Stability Scanning Tunneling Microscope," *IBM J. Res. Develop.* (to be published in Sept. 1986).
- M. Ringger, H. R. Hidber, R. Schlögl, P. Oelhafen, and H.-J. Güntherodt, "Nanometer Lithography with the Scanning Tunneling Microscope," *Appl. Phys. Lett.* 46, 832 (1985).
 M. A. McCord and R. F. W. Pease, "Lithography with the
- M. A. McCord and R. F. W. Pease, "Lithography with the Scanning Tunneling Microscope," J. Vac. Sci. Technol. B4, 86 (1986).

Received November 6, 1985; accepted for publication January 30, 1986

G. Binnig IBM Corporation, Zurich Research Laboratory, Säumerstrasse 4, 8803 Rüschlikon, Switzerland. Dr. Binnig is an IBM Fellow and manager of scanning tunneling microscopy and spectroscopy at the IBM Zurich Research Laboratory. Dr. Binnig received his Ph.D. in experimental physics in 1978 from the Wolfgang Goethe University in Frankfurt a.M., BRD, with an emphasis on superconductivity, and subsequently joined IBM at the Zurich Research Laboratory. His initial efforts at IBM were on the development of the scanning tunneling microscope, for which he received two IBM Outstanding Contribution Awards, the Physics Prize of the German Physical Society in 1982, and the Otto Klung Prize in 1983. He was also corecipient of the Hewlett Packard Prize of the European Physical Society, the King Faisal International Prize for Science in 1984, and an IBM Corporate Award in 1985. During 1985, Dr. Binnig was on leave at the IBM San Jose Research Laboratory and Stanford University.

H. Rohrer IBM Corporation, Zurich Research Laboratory, Säumerstrasse 4, 8803 Rüschlikon, Switzerland. Dr. Rohrer is senior manager of the scanning tunneling microscopy effort at the IBM Zurich Research Laboratory. Dr. Rohrer received his Ph.D. in experimental physics in 1960 from the Eidgenossische Technische Hochschule (ETH) in Zurich, with an emphasis on superconductivity. After a two-year postdoctorate at Rutgers University, New Jersey, he joined IBM in 1963 at the Zurich Research Laboratory. His research interests included Kondo systems, phase transitions, and multicritical phenomena prior to his present work on scanning tunneling microscopy. He spent a sabbatical at the University of California at Santa Barbara in 1974-75. He received an IBM Outstanding Contribution Award for his work on critical phenomena and an IBM Outstanding Innovation Award for his work on the scanning tunneling microscope. In 1984, Dr. Rohrer was corecipient of the Hewlett Packard Prize of the European Physical Society and the King Faisal International Prize for Science, and, in 1985, corecipient of an IBM Corporate Award.